Journal of Applied Sciences and Nanotechnology, Vol. 2, No. 4 (2022)

Journal of Applied Sciences and Nanotechnology

Journal homepage: https://jasn.uotechnology.edu.iq/

2D Particle-in-Cell/Monte Carlo Collision Simulation of Zn-C Mosaic Target Erosion

[1]Ali J. Addie*, [2]Raid A. Ismail, [2]Mudhafar A. Mohammed
[1]Center of Advanced Materials, Ministry of Science and Technology – Iraq
[2]Department of Applied Sciences, University of Technology – Iraq

Article information
Article history:
Received: August, 11, 2022
Accepted: September, 05, 2022
Available online: December, 10, 2022

Keywords:
Mosaic targe erosion,
PIC/MCC analysis,
Magnetron spurting simulation,
Nanohybrid thin films

Corresponding Author:
Ali J. Addie
ali.jaddie@yahoo.com

Abstract
In this work, a simulation analysis of a commercial magnetron sputtering source was performed using the finite element method Particle-in-Cell/Monte Carlo Collision (PIC/MCC) to optimize the configuration of the Zn-C mosaic target. The magnetic field distribution was solved in a two-dimensional cylindrical coordinate system, and particles such as electrons, atoms, and charged ions of argon, zinc, and carbon were tracked in a DC magnetron sputtering system. The sputtering yield profile and particle flux for the eroded target were studied considering the ion and electron density distributions. The maximum sputtering flux of zinc and carbon was 1.975×10^{21} $m^{-2}.s^{-1}$ and 3.7×10^{18} $m^{-2}.s^{-1}$ respectively. The erosion position of a target was predicted based on the maximum power density distribution at the surface of the target. The accuracy of the simulation was checked by comparing it with the measurement of the target eroded after several hours of sputtering. However, as for the Zn-C mosaic target, the racetrack was identical to the analysis predicted by the numerical simulation process. The results of this work can be used as a guide for designing mosaic targets and optimizing their use for fabricating nanohybrid thin film structures.

DOI: 10.53293/jasn.2022.5395.1185, Department of Applied Sciences, University of Technology

1. Introduction

The technical requirements of modern photoelectric applications have increased interest in the fabrication of thin films with specific optical, electrical, mechanical, and surface wetting properties. Currently, there is a growing trend to synthesize films that are single-layer nanohybrid composites that can meet these requirements [1–5]. The properties of films can be further modified by changing their thickness or using complex multilayer heterostructures based on superlattices and gradient structures [6–9]. These nanohybrid compounds consist of several components and are based on oxides, nitrides, or carbides. They are usually dielectric materials that are very difficult to synthesize by sputtering techniques. Deposition of multicomponent thin films is traditionally achieved by RF magnetron sputtering [10, 11]. This technique allows the sputtering of targets from multicomponent dielectric materials. The relatively low productivity of this technique, the high cost of RF power sources, and the complexity of scaling are all drawbacks that affect the potential of this technique for industrial applications. In this context, the reactive sputtering technique is more promising [12–14]. This technique retains all the advantages of magnetron sputtering, including high deposition rate of layers, low substrate temperature, and ease of assembly. It enables the deposition of layers using targets that can be fabricated relatively easily. Thin

multicomponent layers are deposited using three main magnetron sputtering techniques: sputtering with multiple targets, single sputtering of each component, and mosaic targets. When it is possible to obtain an alloy or a mixture of the required elements, the alloy target sputtering method gives excellent results. The composition of the deposited layers almost matches the element concentrations of the original target. However, in some cases, the composition of the deposited layers consists of different materials with limited mutual solubility or large variations in melting temperature. Here, it is extremely difficult to obtain targets with the desired composition. In this case, multitarget sputtering leads to favorable results. In this approach, multiple sputtering sources are used to create multicomponent layers, with each element deposited with a single magnetron [13, 15]. With multitarget sputtering, the elemental composition of the deposited layers can be precisely controlled. Different layers may be created by adjusting the current or discharge capacitance of each magnetron. However, due to its complexity, this technique is rarely used in industrial applications [16]. A new trend in the development of magnetron sputtering technology for the deposition of multicomponent thin films is the use of so-called composite or mosaic targets, i.e., targets consisting of a matrix of one metal with inserts of other metals [17–19]. With a single magnetron, it is possible to create multicomponent layers with any amount and composition of components. The technique of magnetron sputtering of mosaic targets is particularly advantageous when the desired layers are made of materials with poor mutual solubility or large differences in melting temperature. Since the sputtering rate of the substrate and inserts depends on several factors, such as the distribution of the ion current density, the sputtering coefficient of an element, the energy of the ions, etc. The disadvantage of the above method is the complexity of selecting the size and number of inserts to achieve the required concentration and uniform distribution of elements in the deposited layer. Several sputtering experiments on the mosaic target are required, followed by adjusting the size of the inserts based on the results of the elemental analysis of the deposited layers to achieve the appropriate elemental ratio. This selection method is expensive (especially if the target contains rare elements) and time consuming. In this case, computer simulation significantly reduces development time and cost and eliminates errors. Several research papers have addressed the modelling and simulation of the magnetron sputtering process, some with reactive sputtering systems and others with target erosion processes [20–23]. However, magnetron sputtering of mosaic targets has been the subject of relatively few studies, as there is no published work on a numerical method using particle-in-cell/Monte Carlo collision simulation (PIC /MCC), which has been used extensively to study the fundamental process of a static plasma discharge [24–26]. Therefore, the aim of this study is to simulate the sputtering process of mosaic targets using PIC /MCC method to determine the size and position of inserts to correct the composition of the deposited nanohybrid film.

2. PIC/MCC Simulation

Simulation analysis for single and composite targets was adopted in this work to overcome the difficulties in developing the mosaic target. Simulation of mosaic target sputtering can help to determine the size and position of the inserts to best control the composition of the deposited hybrid film. The simulation was performed using the simulation software PEGASUS [27]. The core of the software is based on the particle-in-cell method (PIC) to calculate the motion of charged particles and to determine the distribution of electromagnetic fields. The analysis of the collisions of electrons, ions and neutral species in the plasma is performed using the Monte Carlo collision method (MCC). Together with the flux of electrons and ions on the surface of the target, the spatial distributions of velocity, potential, temperature, density, and flux of electrons and ions in the space above the planar surface of the target exposed to Ar plasma were calculated. Figure 1 shows a schematic representation of the magnetron source used in this simulation. The simulation domain has cylindrical symmetry about the axis r=0, the distance between the sputtering target and the opposing substrate is 33 mm, and the target is a planar disk with a radius of r=25 mm. Two coaxial permanent magnets located under the target generate the magnetic field. The magnetic field is calculated using the finite element method (FEM) according to the experimental configuration. The simulation process includes three main steps: simulation of the plasma dynamics, estimation of the sputtering yield of the target corresponding to the ion bombardment, and finally tracking the movement of the sputtered ions from the target to the substrate. The electric field is calculated by the finite difference method, and the boundary conditions are applied to the right and left sides. On the substrate, the electrostatic potential was neglected, and a DC voltage of 400 V is applied to the target. Based on the simulation results, the mosaic target was designed and fabricated in the laboratory. Later, the target was used to fabricate hybrid thin films on glass and silicon substrates under optimized sputtering conditions. Figure 1a shows that the distance between the target and the substrate is 33 mm. The width of the magnet is 22.8 mm for the S pole and 5.6 mm for the N pole. The distance from the center of the

two poles is 21.3 mm. The chamber is filled with argon gas, the pressure is 1×10^{-2} mbar and the temperature is 300 K.

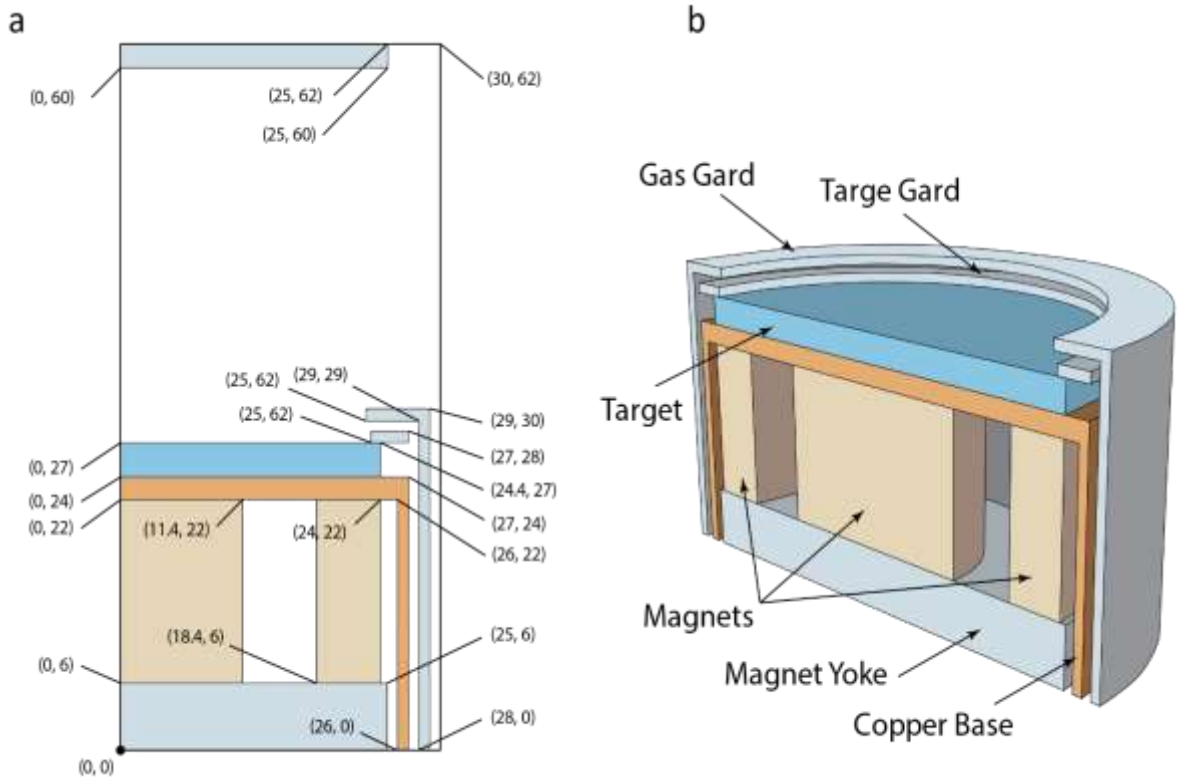

Figure 1: a) Schematic diagram of the magnetron source used in the simulation. All dimensions are in mm. b) cross-section of the 3D design of the magnetron source showing the target and the magnets.

3. Results and Discussion

Permanent magnets trap electrons from the plasma along magnetic flux lines in the magnetron sputter source. These trapped electrons ionize the neutral atoms and generate more plasma particles. Therefore, the magnetic field distribution in a magnetron source is of critical importance. The magnetic field profile is related to the plasma properties and the erosion pattern of the target. An analytical solution for the behavior of the plasma is not easy to find due to the complexity of the magnetic field. The properties of the plasma in a 2D geometry under a constant magnetic field have been studied. Although the numerical solution with higher dimensions is more suitable for the simulation of magnetron sputtering, the symmetry of this configuration can lead to reasonable analytical results. The calculated magnetic field data are shown in Figure 2. The zone where the magnetic field lines are parallel to the target (B=0) is at a radius of r_o=0 cm. The structure of a DC magnetron sputtering system simulated for this work is also shown in the figure. a permanent magnet with a target on one side and a substrate on the other. The simulation domain in the cylindrical 2D coordination is the rectangular region bounded by the solid line. Since the magnetic field induced by the plasma motion is so small, only the static magnetic fields are considered. The color gradient bar value is proportional to the magnetic field strength B. The magnetic flux density generated by the permanent magnet was calculated using commercial software. The magnetic field profile estimated by FEM is used as input data to calculate the particle motion in the simulation of PIC-MCC. Figures 2a and b show the distribution of magnetic field strength. The color contours show the gradient of the field strength, and the solid lines represent the isolines of the strongest regions. The maximum field strength on the surface of the target is about 0.05 T

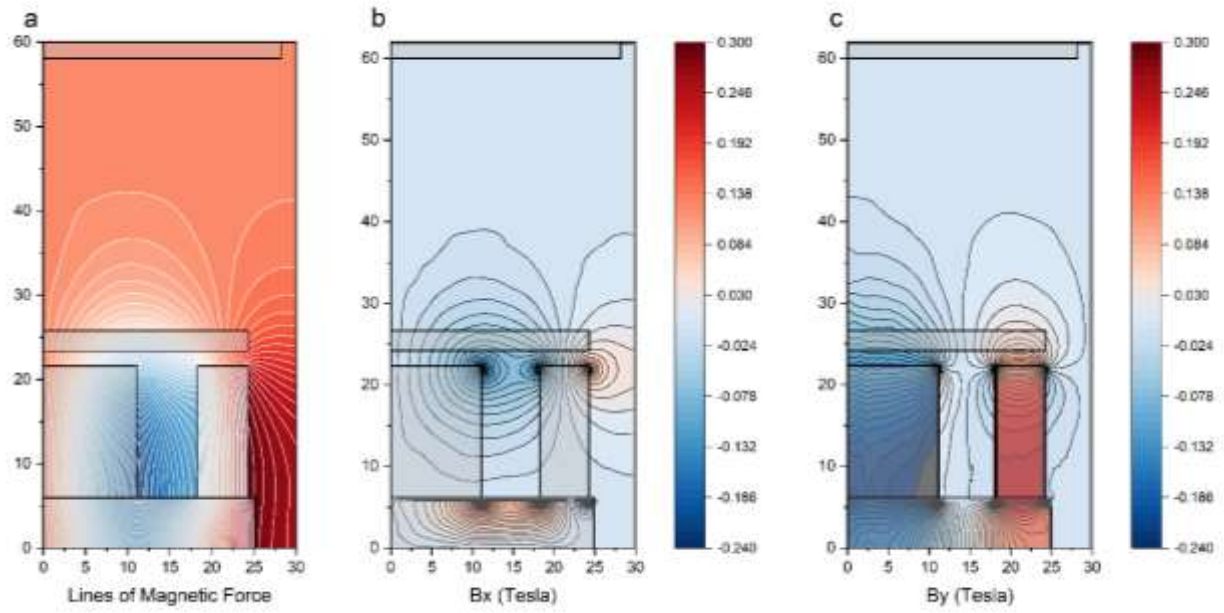

Figure 2: 2D simulation of the magnetic field inside the chamber of the magnetron source. a) distribution of magnetic force lines around the target. b) contours of the magnetic field strength component Bx. c) contours of the element of the magnetic field strength By. All y- and x- axes are in mm

On the other hand, the strong magnetostatic field confines the electrons within the plasma. At magnetic fields of a few Tesla, the electrons typically have gyro radii of a few millimetres and tend to swirl above the target [28, 29]. However, since their gyro radii are of the same order of magnitude as the characteristic length of the magnetic field, their orbits are not perfectly helical, though. This allows electrons to ionize a series of Ar atoms ($e+Ar \rightarrow 2e+Ar^{+}$) until they escape confinement or consume all their kinetic energy, and they contribute to the population of electron density in the plasma. Ar^{+} ions are thus largely produced in the confinement zone generated by the magnetic field. Because of their much larger mass, their radii of gyration at magnetic field strengths are only a few meters. Consequently, their response to the magnetic field is limited on the length scale of the magnetron, and their trajectories deviate only slightly from the electric field lines. Assuming that the electric field acts approximately perpendicular to the surface of the target, it may be expected that the ions fall normally on the surface of the target. The ion bombardment generates the secondary electron emission flux required to sustain the process, and additionally sputters atoms of the deposition material off the target. Magnetic mirror effect increases plasma density in magnetron sputtering when magnetic flux lines are parallel to the target surface. Because ionization occurs in an area of high electron density, the density distribution of argon ions is identical to that of electrons. However, argon ions are not magnetized with 0.5 T. Figure 3 shows the argon-ion and electron densities distribution and generation rate inside the plasma chamber. At first glance, it looks like the density of the ion distribution is the same as the density of the electron distribution. However, there is a slight difference between the two. The highest density of the electron distribution (Figure 3a) was about 2.485×10^{17} m^{-3}, while the highest density of the Ar^{+} distribution (Figure 3c) was slightly higher, at about 2.53×10^{17} m^{-3}. It is also clear from the two figures that the density of the Ar^{+} distribution increases more near the cathode region. The reason for this is the effect of the bias voltage applied at the cathode, which slightly attracts positive ions toward the surface. On the other hand, in both Figures 3b and 3b, we note that the generation rate of ions and electrons is identical because the generation comes from the same ionization event. This equality is justified in these types of low temperature plasmas where the energy is insufficient to cause higher ionization states [30]. The magnetic field effectively confines the electrons. It increases with decreasing distance from the substrate. Higher ion density leads to higher charge density and higher power density at the surface. The figure shows that the highest electron and ion density is cantered directly above the surface of the target at r=15 mm. At a tolerance of ±1.5 mm, the density decreases by an order of magnitude.

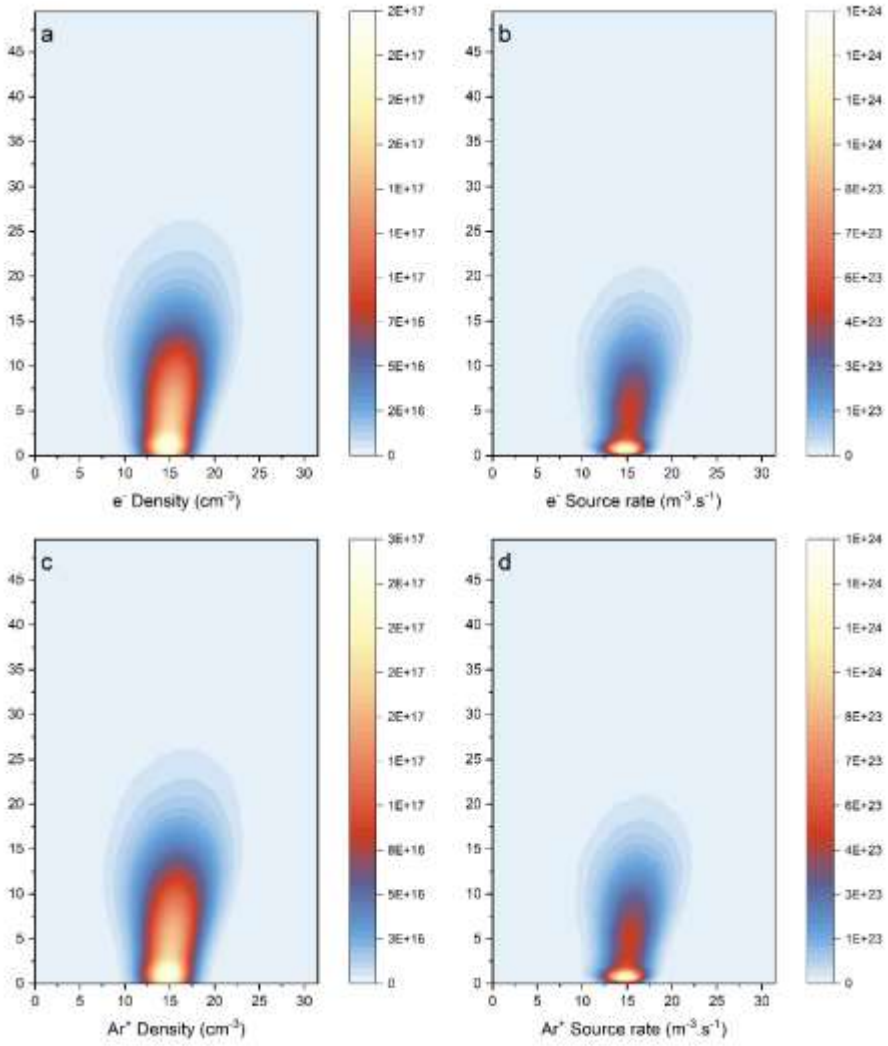

Figure 3: a) 2D simulation of the distribution of the e- density in the vacuum chamber. b) the generation rate of the electrons at the surface of the target. c) ion density distribution and b. the generation rate of the argon ions at the target surface. All y- and x- axes are in mm.

Figure 4 shows the power density distribution above the target surface. The substrate is grounded, and the target is negatively biased. There is a potential difference of about 400 V between the target and the substrate. The power density distribution is allocated at a very narrow region that extends for only about 10 mm at the surface of the target. If we try to find the area of highest power that does not decrease below 1×10^5 W/m^2, the area will be about 3 mm in width centered at r=15 mm from the center of the targe. This is adapted to the design and construction of the mosaic target by choosing a ga graphite insert with a diameter of 3 mm. To investigate the behavior of the proposed mosaic target on the sputtering parameters, the boundary conditions and the design of the system domain have been recalculated by considering a modified design of the target, a composite of two materials consisting of a zinc matrix and graphite inserts. Figure 5. shows the distribution of the sputtered carbon and zinc atoms, the flux of each, and the mean free path for both particles. Zinc has an extremely high sputtering yield, and it may be accounted for among the highest value of all metals [31, 32]. In contrast, carbon has an exceptionally low sputtering yield, resulting in a deposition rate as low as 0.1Å/s, which is highly dependent on the chemical nature of carbon and the deposition process parameters. The figure presents the simulation results of the analytical formula illustrated in Figure 1 for the sputtered target particles estimated using the argon-ion bombardment on the zinc and graphite targets. The spatial distribution of the carbon atom density was significantly lower than that of the zinc atom density by about two orders, making the sputtering from such a combination of the elements extremely sophisticated.

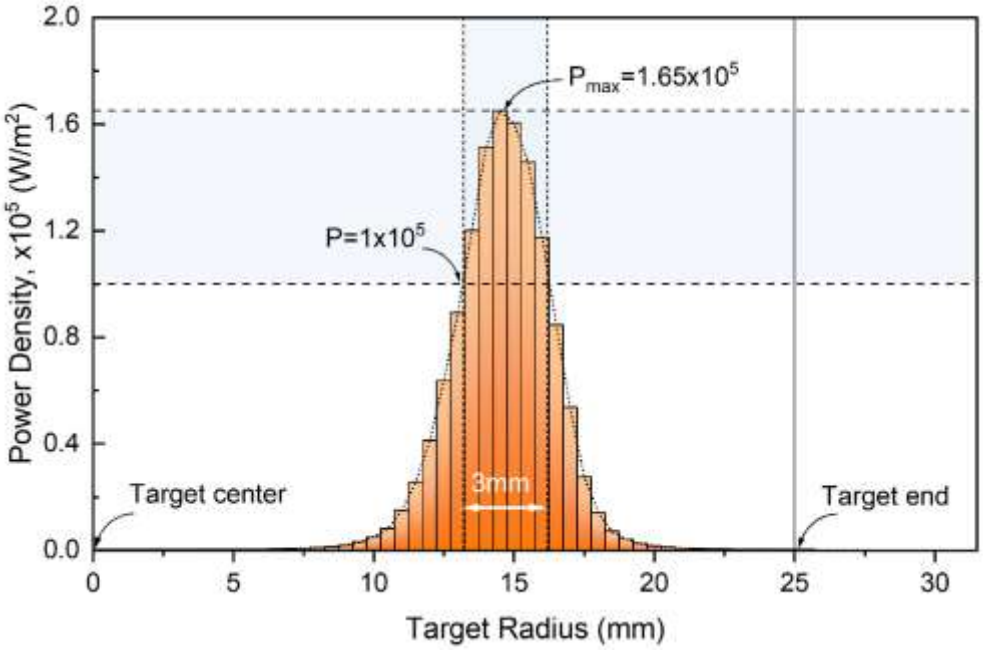

Figure 4: Power density distribution at the surface of the target. The x-axis represents the distance from the center of the target.

The flux of zinc is domination the sputtering process, and it is predicted that the concentration of carbon in the hybrid film will be minimal. Thus, the total amount of ejected particles by the argon ions almost consists of zinc and a small amount of carbon. The number of sputtered particles is determined by the argon ion flux and the energy governed by the voltage applied to the magnetron source and the kind of power used. There is no significant difference in the mean free path for Zn and C atoms; the average value was around 14 mm and 12 mm, respectively. Therefore, the ejected particles will suffer from a multi-collision process before reaching the substrate, losing some energy, and extending diffusion time to be deposited at the substrate surface. Because of the prolonged multi-collision process, the probability of particle clustering in the gas phase will be high, and this will be preferred in the synthesis of nanohybrid thin film structures. The erosion profile can be imagined as an inverse for the sputtering flux of the particles from the target surface. Figure 6. show the simulation of the sputtered flux distribution for the zinc and carbon. The inset is an image of a quarter part of the laboratory mosaic target showing the position of the graphite inserts. There were 16 graphite inserts with diameter of 3 mm distributed at r=15 mm from the center of the target. For illustration purpose the flux of C atoms was multiplied several times as their magnitude is much lower than the Zn flux (3 orders higher for the Zn flux). The major disadvantage of this design is the inhomogeneous target erosion due to the differences in the sputter yield of the base zinc target and the inserted graphite material. According to the simulation analysis the erosion of the target will concentered around the graphite inserts and the validity of the simulation results have experimentally proved. The most collisions between free electrons and argon atoms and hence ions created are located at the r=15 mm. The distribution of ions and hence majority of the sputtering are gathered at this radius. As demonstrated in Figure 7, spatially dependent erosion produces a ring or "racetrack" devoid of target material. The target power and magnetic field intensity determine the shape of the erosion pattern. An increase in magnetic field strength will narrow the racetrack, but an increase in cathode voltage would widen it [33–35]. Once the depth of the racetrack approaches the thickness of the target, the target cannot be used without risk of damaging the magnetron source or introducing contaminants into the deposited film. The pattern of erosion can limit the use of sputtering targets to a small percentage of their original mass.

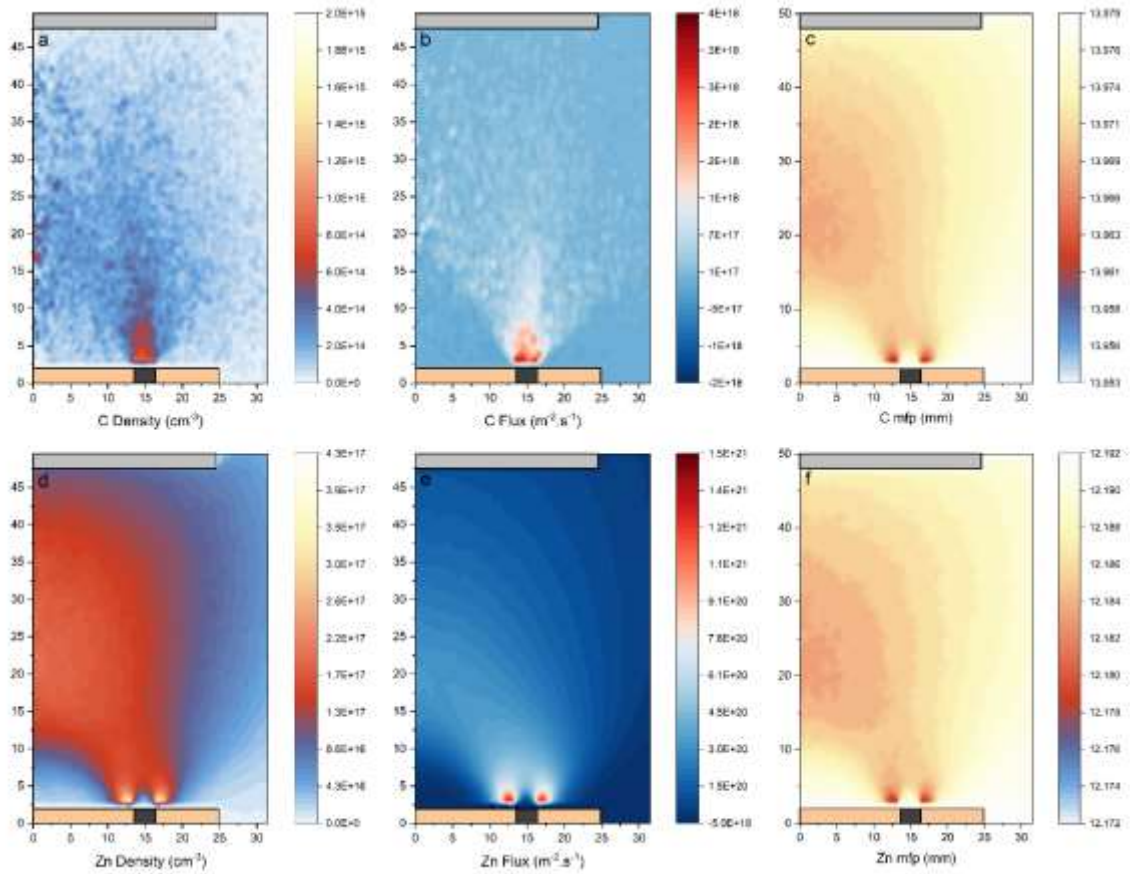

Figure 5: 2D simulation of the density of sputtered atom, the flux of particles, and mean free path for the sputtered C atoms (subfigures a, b, and c, respectively) and for sputtered Zn atoms (subfigures d, e, and f, respectively). All y- and x- axes are in mm.

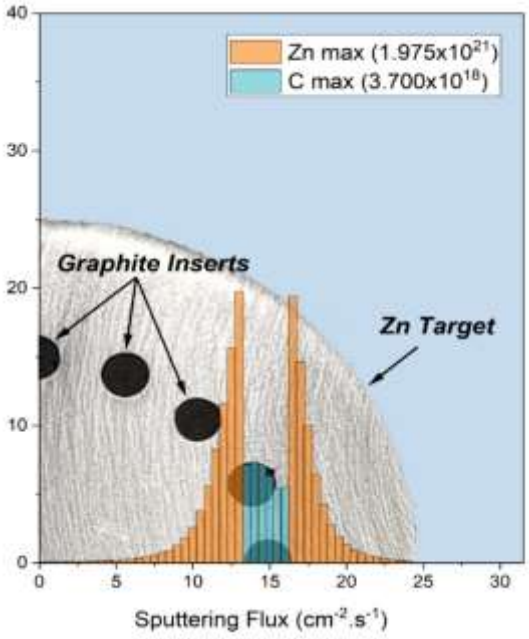

Figure 6: Simulation of the sputtered flux distribution for the zinc and carbon. The inset represents the photo for the mosaic target showing the position of the graphite inserts. Both y- and x- axes are in mm.

The accuracy of the simulation was verified by comparison with measurement of target eroded after several sputtering hours (Figure 7). Both Zn and graphite target developed normal magnetron target erosion profile, despite that the zinc target show deeper erosion track compared with graphite target. The behavior agrees well with the simulation analysis, as the Zn have extremely higher sputtering flux whereas C have exceptionally low sputtering flux. The influence of carbon redeposition could be readily recognized in the center of the mosaic target, where a negative erosion rate was assumed which means a layer had grown there. Although, as for the mosaic target the racetrack was identical with predicted analysis produced by simulation process.

Figure 7: Mosaic targets used in experiments show the erosion of the surface after several hours of operation.

4. Conclusions

Simulation analysis of a magnetron sputter source was performed using the finite element method Particle-in-Cell/Monte Carlo Collision (PIC /MCC) to optimize the configuration of the mosaic target. The simulated and fabricated mosaic target can be used for the deposition of nanohybrid Zn/C films. According to the simulation results, the flux of Zn atoms was three orders of magnitude higher than the flux of C atoms. The accuracy of the simulation was verified by comparing it with the measurement of the target eroded after hundreds of sputtering hours. However, as with the mosaic target, the racetrack was identical to the analysis predicted by the numerical simulation.

Conflict of Interest

The authors declare that they have no conflict of interest.

References

[1] L. Yao and J. He, "Recent progress in antireflection and self-cleaning technology - From surface engineering to functional surfaces," *Progress in Materials Science*, vol. 61, pp. 94–143, 2014, doi: 10.1016/j.pmatsci.2013.12.003.

[2] B. S. Nugroho, *Optical Response of Nanohybrids: Effects of Exciton-Plasmon Interaction*. 2016.

[3] Z. T. Wang, J. L. Xu, H. Zhou, and X. Zhang, "Facile synthesis of Zn(II)-doped g-C 3 N 4 and their enhanced photocatalytic activity under visible light irradiation," *Rare Metals*, no. Ii, 2019, doi: 10.1007/s12598-019-01222-5.

[4] S. Byun, B. Shin, and J. Yu, "Metal sputtered graphene based hybrid films comprising tin oxide/reduced graphene oxide/Ni as electrodes for high-voltage electrochemical capacitors," *Carbon*, vol. 129, pp. 1–7, 2018, doi: 10.1016/j.carbon.2017.11.098.

[5] A. Purabgola and B. Kandasubramanian, *Thin films for planar solar cells of organic-inorganic perovskite composites*. Elsevier Ltd., 2021. doi: 10.1016/b978-0-12-819977-0.00003-2.

[6] J. C. Blancon, J. Even, C. C. Stoumpos, M. G. Kanatzidis, and A. D. Mohite, "Semiconductor physics of organic–inorganic 2D halide perovskites," *Nature Nanotechnology*, vol. 15, no. 12, pp. 969–985, 2020, doi: 10.1038/s41565-020-00811-1.

[7] A. Ganose, *Atomic-scale insights into emergent photovoltaic absorbers*. 2018.

[8] S. Yu, C. Chen, H. Zhang, J. Zhang, and J. Liu, "Design of high sensitivity graphite carbon nitride/zinc oxide humidity sensor for breath detection," *Sensors and Actuators, B: Chemical*, vol. 332, no. January, p. 129536, 2021, doi: 10.1016/j.snb.2021.129536.

[9] R. Singh and R. Bhateria, "Core–shell nanostructures: a simplest two-component system with enhanced properties and multiple applications," *Environmental Geochemistry and Health*, vol. 43, no. 7, pp. 2459–2482, 2021, doi: 10.1007/s10653-020-00766-1.
[10] P. N. Tri, S. Rtimi, and C. M. O. Plamondon, *Nanomaterials-based coatings: Fundamentals and applications*. 2019. doi: 10.1016/C2017-0-03415-8.
[11] D. M. Mattox, *Handbook of Physical Vapor Deposition (PVD) Processing*. Elsevier, 2010. doi: 10.1016/C2009-0-18800-1.
[12] N. K. T. Bui, "Growth of earth abundant material based thin films by sputtering technique for photovoltaics," 2022.
[13] A. Baptista, F. Silva, J. Porteiro, J. Míguez, and G. Pinto, "Sputtering physical vapour deposition (PVD) coatings: A critical review on process improvement andmarket trend demands," *Coatings*, vol. 8, no. 11, 2018, doi: 10.3390/COATINGS8110402.
[14] D. Yu *et al.*, "Microstructure, mechanical and tribological properties of TaCN composite films by reactive magnetron sputtering," *Ceramics International*, vol. 46, no. 13, pp. 20683–20694, 2020, doi: 10.1016/j.ceramint.2020.04.205.
[15] B. Braeckman, "Sputter Deposition of Complex Alloy Thin Films," 2017.
[16] J. E. Greene, "Review Article: Tracing the recorded history of thin-film sputter deposition: From the 1800s to 2017," *Journal of Vacuum Science & Technology A: Vacuum, Surfaces, and Films*, vol. 35, no. 5, p. 05C204, 2017, doi: 10.1116/1.4998940.
[17] N. Witit-Anun and A. Buranawong, "Effect of substrate-target distance on the structure of TiCrN films deposited from mosaic target by reactive DC magnetron sputtering," *Key Engineering Materials*, vol. 798 KEM, pp. 163–168, 2019, doi: 10.4028/www.scientific.net/KEM.798.163.
[18] N. Witit-anun, A. Buranawong, and S. Chaikhun, "Effect of nitrogen flow rate on structure of TiCrN thin films prepared from mosaic target by reactive dc unbalanced magnetron sputtering," *Phranakhon Rajabhat Research Journal (Science and Technology)*, vol. 13, pp. 38–49, 2018.
[19] X. Feng, K. Zhang, Y. Zheng, H. Zhou, and Z. Wan, "Chemical state, structure and mechanical properties of multi-element (CrTaNbMoV)Nx films by reactive magnetron sputtering," *Materials Chemistry and Physics*, vol. 239, no. August 2019, p. 121991, 2020, doi: 10.1016/j.matchemphys.2019.121991.
[20] R. V. Bogdanov and O. M. Kostiukevych, "Computer simulation of sputtering of graphite target in magnetron sputtering device with two zones of erosion," *Materials Science- Poland*, vol. 33, no. 1, pp. 82–94, 2015, doi: 10.1515/msp-2015-0001.
[21] T. Nyberg, H. Högberg, G. Greczynski, and S. Berg, "A simple model for non-saturated reactive sputtering processes," *Thin Solid Films*, vol. 688, no. April, p. 137413, 2019, doi: 10.1016/j.tsf.2019.137413.
[22] Y. peng He, S. bo Bi, J. ping Yin, S. bo Lv, R. sheng Wang, and Z. Lin, "Prediction of midfrequency sputtering cathode erosion position with vertical magnetic field," *Surface Engineering*, vol. 37, no. 3, pp. 381–389, 2021, doi: 10.1080/02670844.2020.1747752.
[23] V. I. Shapovalov, H. Ahmedov, A. A. Kozin, A. Demir, and B. Korutlu, "Simulation of the effect of argon pressure on thermal processes in the sputtering unit of a magnetron with a hot target," *Vacuum*, vol. 192, no. June, p. 110421, 2021, doi: 10.1016/j.vacuum.2021.110421.
[24] K. Singh, "Proposition of a model for prediction of coating composition deposited by reactive magnetron sputtering and its experimentation validation on Nb-Ti," *International Journal of Applied Engineering and Technology*, vol. 4, no. 2, pp. 25–41, 2014.
[25] D. A. Golosov, S. N. Melnikov, and A. P. Dostanko, "Calculation of the Elemental Composition of Thin Films Deposited by Magnetron Sputtering of Mosaic Targets," vol. 48, no. 1, pp. 52–59, 2012, doi: 10.3103/S1068375512010073.
[26] A. E. Komlev, E. S. Shutova, and A. A. Komlev, "Features of magnetron sputtering of a doubled Ta/Ti target," *IOP Conference Series: Materials Science and Engineering*, vol. 387, no. 1, pp. 3–7, 2018, doi: 10.1088/1757-899X/387/1/012038.
[27] M. W. Kunz, J. M. Stone, and X. N. Bai, "Pegasus: A new hybrid-kinetic particle-in-cell code for astrophysical plasma dynamics," *Journal of Computational Physics*, vol. 259, pp. 154–174, 2014, doi: 10.1016/j.jcp.2013.11.035.
[28] Q. I. U. Qingquan *et al.*, "Simulation to predict target erosion of planar DC magnetron," *Plasma Science and Technology*, vol. 10, no. 5, pp. 581–587, 2008, doi: 10.1088/1009-0630/10/5/12.
[29] J. Musschoot and J. Haemers, "Qualitative model of the magnetron discharge," *Vacuum*, vol. 84, no. 4, pp.

488–493, 2009, doi: 10.1016/j.vacuum.2009.10.011.
[30] A. Piel, *Plasma Physics*. Cham: Springer International Publishing, 2017. doi: 10.1007/978-3-319-63427-2.
[31] R. Schelfhout, K. Strijckmans, and D. Depla, "Sputter yield measurements to evaluate the target state during reactive magnetron sputtering," *Surface and Coatings Technology*, vol. 399, p. 126097, Oct. 2020, doi: 10.1016/j.surfcoat.2020.126097.
[32] P. M. Martin, *Handbook of Deposition Technologies for Films and Coatings*, vol. 7. Elsevier, 2010. doi: 10.1016/B978-0-8155-2031-3.00021-1.
[33] Y. Ohtsu, S. Tsuruta, T. Tabaru, and M. Akiyama, "Plasma characteristics and target erosion profile of racetrack-shaped RF magnetron plasma with weak rubber magnets for full circular target utilization," *Surface and Coatings Technology*, vol. 307, pp. 1134–1138, 2016, doi: 10.1016/j.surfcoat.2016.03.003.
[34] K. Strijckmans and D. Depla, "Modeling target erosion during reactive sputtering," *Applied Surface Science*, vol. 331, pp. 185–192, 2015, doi: 10.1016/j.apsusc.2015.01.058.
[35] Q. H. Fan, D. Galipeau, L. Q. Zhou, and J. J. Gracio, "Computer-aided development of a magnetron source with high target utilization," *Vacuum*, vol. 85, no. 8, pp. 833–838, 2011, doi: 10.1016/j.vacuum.2010.12.007.